Flow Pulsations on Concave Conic Forebodies

L. E. Ericsson*
Lockheed Missiles & Space Company, Inc., Sunnyvale, Calif.

A simple mathematical model has been developed for predicting the frequency of the pulsatory flow phenomenon observed on forebodies of concave conic shape; for example, a body with a flow separation spike. It is found that the Strouhal number $S=0.2$ defines an upper limit for the oscillation frequency, where the characteristic length is the length of the spike or concave nosetip for long spikes and the maximum forebody diameter for short spikes.

Nomenclature

A = axial force: coefficient $C_A = \dfrac{A}{(\rho_\infty U_\infty{}^2/2)S}$
a = speed of sound
c = reference length $= D$
D = body diameter (Fig. 4)
$\bar{D}$ = reattachment diameter (Fig. 4)
D_F = diameter of flat-face area (Fig. 5)
d_S = spike diameter (Fig. 6)
f = oscillation frequency
$L, \bar{L}$ = spike length definitions (Fig. 6)
L_S = spike length for flat-faced bodies
M = Mach number $= U/a$
p = static pressure
Re = Reynolds number
Re_D = Re based on D and freestream conditions
S = reference area $= \pi c^2/4$
S_D, S_{L_S} = Strouhal number: $S_D = fD/U_\infty$, $S_{L_S} = fL_S/U_\infty$
T = oscillation period
U = axial velocity
X_l = parameter defined in Eq. (19)
ΔC_A = spike-induced axial force reduction
Δ_{sh} = shock standoff distance for body without spike
ϵ = small parameter – see Eq. (7)
θ_c = spike tip cone angle (Fig. 6)
ρ = air density

Subscripts

d = downstream
eff = effective value
l = linear-tangential extension
max. = maximum
S = spike
u = upstream
1 = conditions before shoulder reattachment (Fig. 4)
∞ = freestream condition

Superscripts

$()^*$ = value (hypothetical) for maximum spike length
$\bar{()}$ = overbarred quantities denote integrated mean or time-average values
$\hat{()}$ = caret indicates value behind a normal shock

Presented as Paper 77-1130 at the AIAA 4th Atmospheric Flight Mechanics Conference, Hollywood, Fla., Aug. 8-10, 1977; submitted Oct. 14, 1977; revision received April 6, 1978.

Index categories: Nonsteady Aerodynamics; Supersonic and Hypersonic Flow; Jets, Wakes, and Viscid-Inviscid Flow Interactions.

*Consulting Engineer. Associate Fellow AIAA.

Introduction

THE oscillatory flows observed in the past on spiked-body geometries have become of renewed interest. Ablation and particle erosion can generate concave re-entry body nose geometries, so-called probescidean nose shapes,[1] which experience the flow pulsations observed on bluff bodies with short spikes. The vehicle designer needs to know the amplitude-frequency characteristics of the fluctuating pressure field to assess the adequacy of the structural design. As the energy is almost completely concentrated in a "harmonic spike," determined by the separated flow geometry, it is important to know at what frequency this energy peak will occur. In this paper, simple (analytic) means are developed by which this critical frequency can be predicted.

The sequence of flow pictures obtained by Kabelitz[2,3] in his theoretical and experimental investigation of the unsteady flow on biconic concave nose geometries illustrates the various phases of spike-induced pulsating flow (Fig. 1). Since the time Mair[4] first studied the flow pheonomenon, it has been customary to use the diameter of the blunt face when denoting the dimensionless frequency of the pulsating flow. Although this Strouhal number S_D is useful, Fig. 1 shows rather convincingly that it is the spike length that is the characteristic dimension on which the dimensionless frequency should be based. Early experimental data for varying spike length obtained by Daniels and Yoshihara[5] show that the Strouhal number based on face diameter S_D decreases with increasing spike length (Fig. 2). This is the expected result of the longer time required for the shock to travel a longer distance (with the same velocity). If the shock velocity remained the same, the Strouhal number based on spike length S_{L_S} would be a constant. Figure 3 shows, however, that instead of being constant, S_{L_S} increases with increasing spike length, both at supersonic[5] and hypersonic[6] Mach numbers. This indicates that the shock velocity increases with increasing spike length. That this is the expected result of the changing reattachment conditions for increasing spike length will be shown later.

Discussion

Maull[7] explained the pulsating flow occurrence in the following simple manner. When the flow U_l approaching the body shoulder can be turned by an attached conical shock, a steady flow condition exists (top half of Fig. 4). Maull computed the largest spike length that would allow this attached conic shock for various shoulder radii on the flat cylinder face. He found that this critical geometry agreed rather well with the experimentally established boundary between stable and pulsatory flow.† When the required flow turning angle is larger than what can be accomplished by such

†The flow pulsations are prevented if the shoulder radius exceeds a critical magnitude.

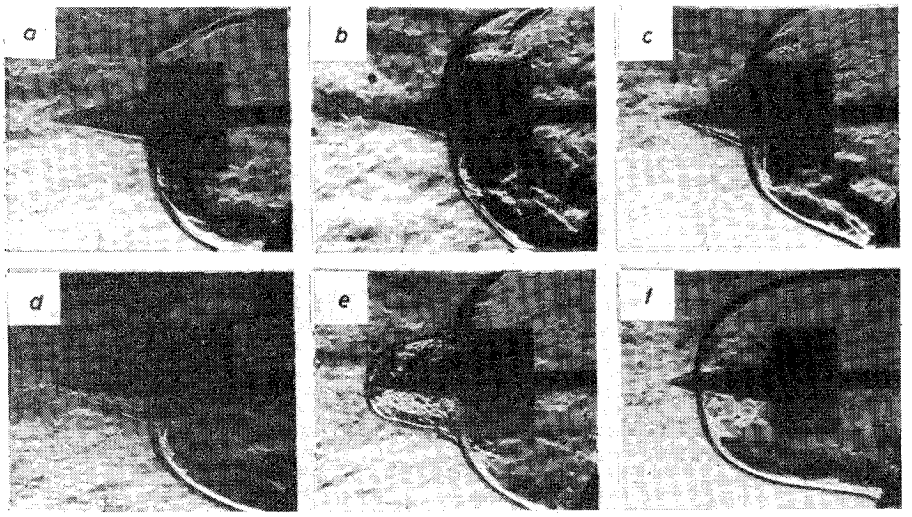

Fig. 1 Spike-induced pulsating flow.[2]

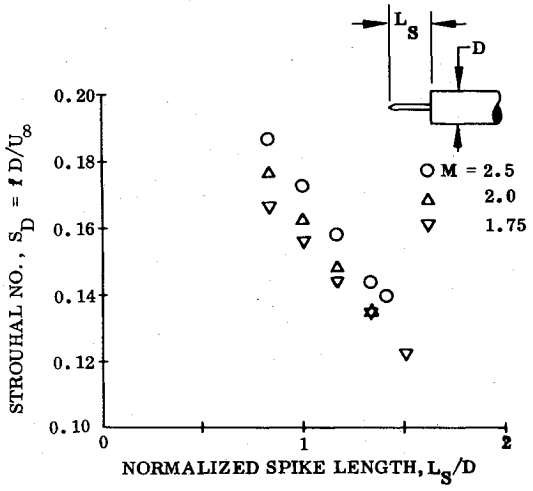

Fig. 2 Effect of spike length on Strouhal number S_D.[5]

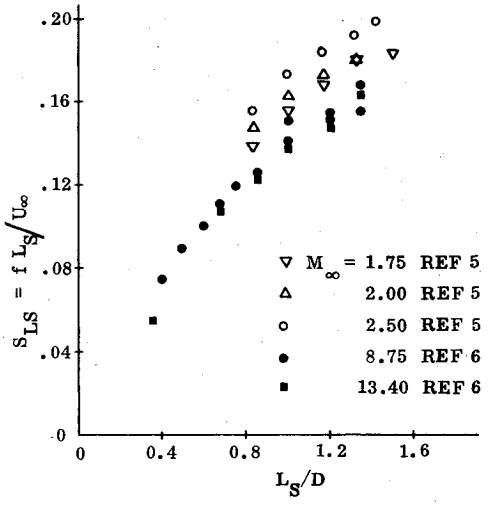

Fig. 3 Effect of spike length on Strouhal number S_{L_S}.

an attached conical shock, a detached strong shock is formed, causing most of the shear layer to be turned back into the recirculatory region (bottom half of Fig. 4). As a result, the recirculatory region starts to grow and the pulsating flow is established.

It may seem overly simplistic to use this purely inviscid flow concept to determine when a viscous flow phenomenon starts. However, Elfstrom[8] has used the same concept to determine when incipient separation starts in high Reynolds number flow; it starts when the required flow turning angle exceeds that allowing an attached oblique or conic shock. Bogdonoff et al.[9] show that Elfstrom's simple inviscid concept agrees better with experimental data than other more involved mathematical models (e.g., Ref. 10). The same simple inviscid flow concept also predicts when shock-induced separation will occur on a delta wing at supersonic speeds; it occurs when the leading edge shock becomes detached, thereby creating an embedded supersonic flow region that is terminated by a normal shock, which usually will be strong enough to cause the boundary layer to separate.[11-13] Kabelitz[2] speculates that the reasoning behind Maull's criterion for flow unsteadiness was that the flow aft of the reattachment shock(s) goes subsonic, which, of course, practically coincides with the shock detachment event.[14] It should be noted that this inviscid criterion is a necessary but not sufficient condition for flow pulsations to occur. In addition, it is required that the Reynolds number based on the free shear layer thickness at reattachment exceeds a critical value (see Ref. 15).

Analysis

Frames b-f in Fig. 1 show how the recirculatory region grows as a result of the free shear layer being turned back into the recirculatory region by the strong (reattachment) shock. When the front of this growing, separated flow region reaches the spike tip, the separation region collapses and is "spilled" downstream over the cylinder shoulder in the form of a ring vortex.[16] The recirculatory flow buildup then starts all over again, as shown in frame a of Fig. 1. Thus, the time period for one cycle of pulsation is composed as follows:

$$T = L_S/\bar{U}_d + L_S/\bar{U}_u \qquad (1)$$

$\bar{U}_u$ is the mean upstream convection velocity of the mass flow added to the recirculatory region by the strong reattachment shock interaction. After reaching the spike tip, the separated flow region is assumed to be "spilled" downstream with slightly less than freestream velocity, i.e., $\bar{U}_d < U_\infty$.

The Strouhal number defined by Eq. (1) is

$$S_{L_S} = \frac{fL_S}{U_\infty} = \frac{\bar{U}_u}{U_\infty}\left[1 + \frac{\bar{U}_u}{U_d}\right]^{-1} \qquad (2)$$

How $\bar{U}_u$ varies with spike length will be determined through the spike efficiency as a forebody drag reducer.[17,18] The stable and unstable flow conditions for a critical spike geometry are illustrated in the top and bottom halves, respectively, of Fig.

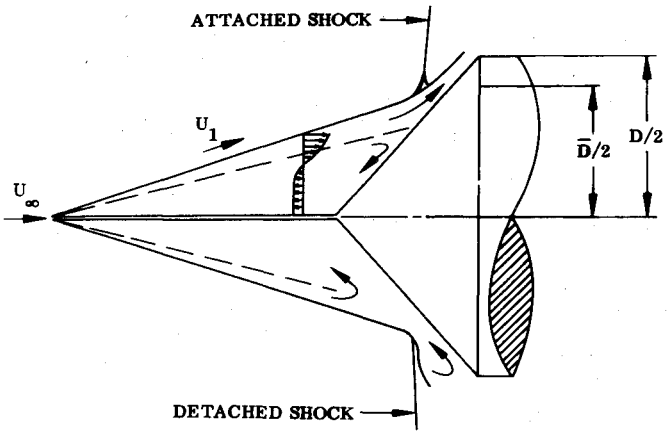

Fig. 4 Steady and unsteady spike-induced separated flow.

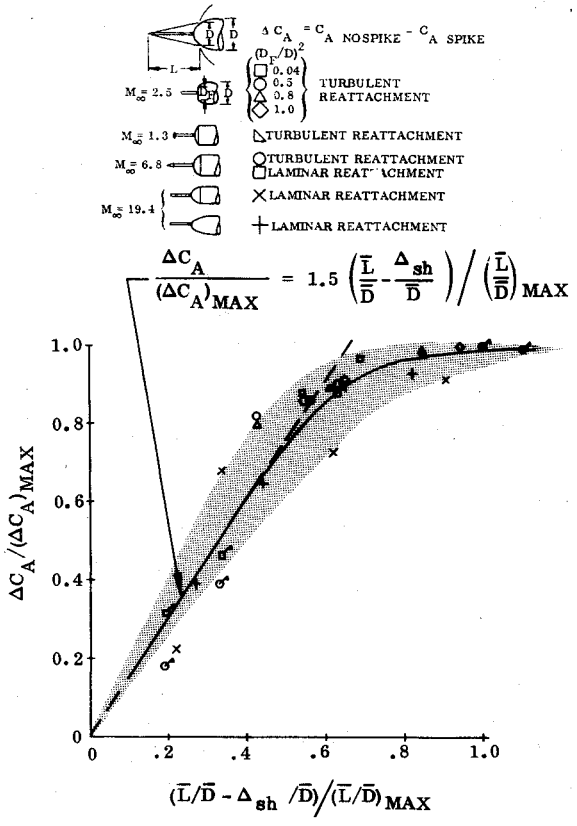

Fig. 5 Spike-induced forebody drag reduction.

4. It is assumed that the velocity $\bar{U}_u$ in Eq. (2) is proportional to the mean convection velocity for the corresponding fictitious steady flow condition. This steady-state convection velocity will decrease with decreasing spike length since the backflow driving pressure rise through the reattachment shock is decreasing. This explains the trend shown by the data in Fig. 3.

The spike-induced drag reduction is

$$\Delta C_A = \frac{\hat{p}_1 - p_1}{(\rho_\infty U_\infty{}^2/2)}\left(\frac{\bar{D}}{D}\right)^2 \tag{3}$$

According to the Chapman-Korst simple theoretical model,[19] $\hat{p}_1$ represents the stagnation pressure for the returning flow. Thus, if $\bar{U}_u$ is of incompressible flow magnitude, Bernoulli's law gives

$$\hat{p}_1 \sim p_1 + \rho \bar{U}_u{}^2/2 \tag{4}$$

From Eqs. (3) and (4), one obtains

$$\bar{U}_u \sim (\Delta C_A)^{1/2} \tag{5}$$

It is assumed that for the spike lengths of interest, the backflow profiles remain similar and $\bar{D}/D$ remains constant, as the reattachment occurs near the shoulder in the pulsating flow case, $\bar{D}/D \approx 1$. The maximum forebody drag reduction, and consequently the maximum frequency, is obtained with the longest spike that will retain flow separation at the spike tip. The ratio between the actual frequency and this maximum value can be expressed through the spike-induced forebody drag reduction. If it is assumed that compressibility effects will not significantly influence the ratio $\bar{U}_u/(\bar{U}_u)_{\max.}$, one obtains

$$\bar{U}_u/(\bar{U}_u)_{\max.} = [\Delta C_A/(\Delta C_A)_{\max.}]^{1/2} \tag{6}$$

which in Eq. (2) gives the following result:

$$\frac{S_{LS}}{(S_{L_S})_{\max.}} = \left(\frac{\Delta C_A}{(\Delta C_A)_{\max.}}\right)^{1/2}(1-\epsilon) \tag{7a}$$

$$1-\epsilon = \left[1+\left(\frac{\bar{U}_u}{\bar{U}_d}\right)_{\max.}\right]\Big/\left(1+\frac{\bar{U}_u}{\bar{U}_d}\right) \tag{7b}$$

In order to obtain information about $\Delta C_A/(\Delta C_A)_{\max.}$, one has to study geometries that allow "steady" flow for the (L_S/D) range of interest. Spiked bodies with spherical shoulders form one such geometric family. The results shown in Figs. 5 and 6 were obtained in an earlier study.[18] For spike lengths giving pulsating flow, the data in Fig. 5 can be represented by the following linear formulation:

$$\frac{\Delta C_A}{(\Delta C_A)_{\max.}} = \frac{3}{2}\left(\frac{\bar{L}}{\bar{D}} - \frac{\Delta_{sh}}{\bar{D}}\right)\Big/\left(\frac{\bar{L}}{\bar{D}}\right)_{\max.} \tag{8}$$

Combining Eqs. (7) and (8) gives

$$\frac{S_{L_S}}{(S_{L_S})_{\max.}} = (1-\epsilon)\left[\frac{3}{2}\left(\frac{\bar{L}}{\bar{D}} - \frac{\Delta_{sh}}{\bar{D}}\right)\Big/\left(\frac{\bar{L}}{\bar{D}}\right)_{\max.}\right]^{1/2} \tag{9}$$

$(\bar{L}/\bar{D})_{\max.}$ is defined as follows by the experimental results in Fig. 6:

$$\left(\frac{\bar{L}}{\bar{D}}\right)_{\max.} = \begin{cases} 1.6(1+0.1M_\infty) & (M_\infty \le 11.3) \\ 3.4 & (M_\infty > 11.3) \end{cases} \tag{10}$$

For tangential flow reattachment‡ on the hemisphere nose, $\bar{L}$ and L in Fig. 6 are related as follows:

$$\left(\frac{\bar{L}}{\bar{D}}\right)_{\max.} = \left\{\left(\frac{L}{D}\right)_{\max.}\left[1+\left(\frac{L}{D}\right)_{\max.}\right]\right\}^{1/2} \tag{11}$$

For flat-faced bodies with thin pointed spikes, $\bar{L}/\bar{D}$ can be substituted with L_S/D. Pulsating flow data for such bodies[5,6] give the results shown in Fig. 7. The data have been normalized to the reattachment condition for the maximum spike length using Eq. (9). The data are seen to scatter around a straight line. The lack of Mach number bias in the data scatter indicates that the compressibility effect in the recirculatory region is indeed negligible. The results in Fig. 7 give

$$(S_{L_S})_{\max.} = 0.26(1-\epsilon) \tag{12a}$$

$$\epsilon = 0.14\,(L_S/D - \Delta_{sh}/D) \tag{12b}$$

‡Although this leads to overestimation of both $\bar{L}$ and $\bar{D}$, it should give a rather good approximation of $\bar{L}/\bar{D}$.

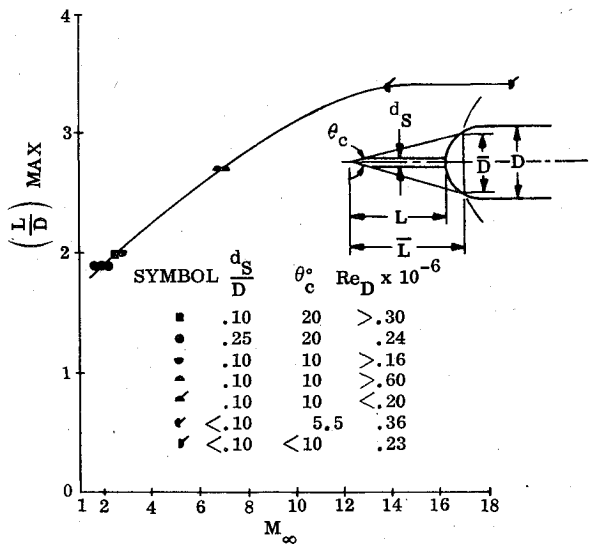

Fig. 6 Spike length for maximum drag reduction as a function of Mach number.

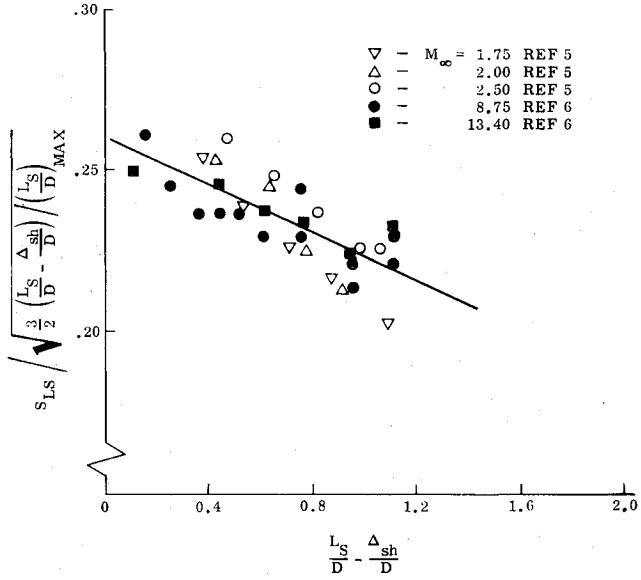

Fig. 7 Normalized Strouhal number of spike-induced pulsating flow.

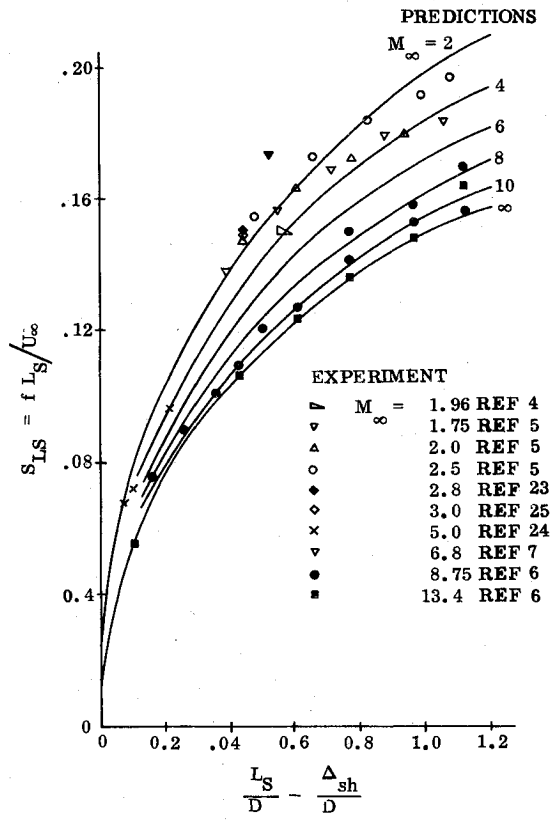

Fig. 8 Comparison between predicted and measured Strouhal numbers of spike-induced flow pulsations.

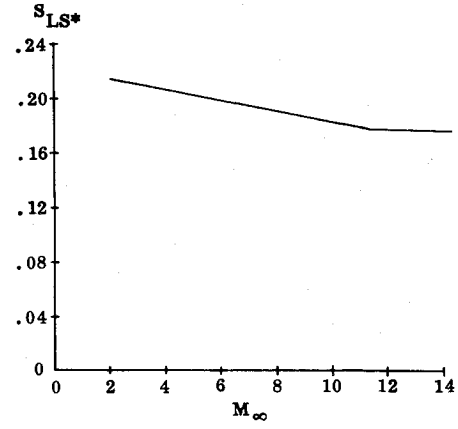

Fig. 9 Maximum Strouhal number of spike-induced pulsating flow.

Combining Eqs. (9) and (12), one obtains

$$S_{L_S} = \frac{0.32}{(L_S/D)_{\max.}^{1/2}}\left[\frac{L_S}{D}-\frac{\Delta_{sh}}{D}\right]^{1/2}\left[1-0.14\left(\frac{L_S}{D}-\frac{\Delta_{sh}}{D}\right)\right] \quad (13)$$

For the bluff geometries producing pulsating flow, a good approximation of the (no spike) shock detachment distance is the following[20]:

$$\Delta_{sh}/D = 0.515(\hat{\rho}/\rho_\infty - 1)^{1/2} \quad (14)$$

where $\hat{\rho}/\rho_\infty$ is the density ratio through a normal shock.

Experimental data from two tests[5,6] had to be used to define $(S_{L_S})_{\max.}$ and ϵ, Eq. (12), as no theoretical means are presently available for computation of these needed flow parameters. That is, the method is semiempirical in nature, like other theoretical methods that deal with boundary-layer flow, with or without the occurrence of flow separation. This condition is likely to persist into the foreseeable future in spite of the availability of bigger and better computers.[21,22] If the mathematical model includes all pertinent physical flow processes, once the needed flow parameters are determined, by a limited test series or otherwise, it should be possible to predict the results obtained in other tests.

Combining Eqs. (10), (13), and (14) gives the S_{L_S} predictions shown in Fig. 8 for $M_\infty = 2$, 4, 6, 8, 10, and ∞. The agreement with available experimental data[4-7,23-25] is generally very good. It is only Maull's single data point[7] that shows any substantial deviation. The reason for this is not known at the present. The results in Fig. 8 are all for pointed thin spikes. If the spike has a blunt tip, e.g., a planar cut, the measured frequencies[20] are higher than predicted. The reason for this is that the reattachment conditions are those corresponding to a longer pointed spike.[15] In this case and when a "hammerheaded" spike tip is used, one needs forebody drag measurements in lieu of Eqs. (10) and (13) for the determination of S_{L_S}.

It is clear that the similar profile assumptions used to derive Eq. (13) are not valid for short spike lengths. When L_S/D exceeds Δ_{sh}/D, the established recirculatory flow region starts

out with a finite upstream convection velocity and not with $\bar{U}_u = 0$, which is the value implied by Eq. (13). That is, the predicted S_{L_S} values in Fig. 8 should be finite, not zero, when $(L_S/D - \Delta_{sh}/D)$ approaches zero. One way to accomplish this is to extend the predictions tangentially below a certain shock penetration value. Judging by the experimental data in Fig. 8, it appears reasonable to make this linear extension for $(L_S/D - \Delta_{sh}/D) \leq 0.25$. Thus, Eq. (13) is modified as follows:

$$S_{L_S} = \frac{0.32}{(L_S/D)^{1/2}_{\max.}} \begin{cases} \left(\frac{L_S}{D} - \frac{\Delta_{sh}}{D}\right)^{1/2}\left[1 - 0.14\left(\frac{L_S}{D} - \frac{\Delta_{sh}}{D}\right)\right] & \left(\frac{L_S}{D} - \frac{\Delta_{sh}}{D} > 0.25\right) \\ 0.26\left[1 + 3.46\left(\frac{L_S}{D} - \frac{\Delta_{sh}}{D}\right)\right] & \left(\frac{L_S}{D} - \frac{\Delta_{sh}}{D} \leq 0.25\right) \end{cases} \tag{15}$$

The similar flow profile assumption also breaks down at the other end of the $(L_S/D - \Delta_{sh}/D)$ range. For deep spike penetration the reattachment conditions approach a constant value, i.e., $\bar{U}_u = \text{constant}$. As $\bar{U}_d = \text{constant}$ also, it follows from Eq. (2) that $S_{L_S} = \text{constant}$. This constant value for large spike lengths, $S_{L_S}{}^*$, is determined as follows. Figure 5 shows that in the linear approximation $\Delta C_A = (\Delta C_A)_{\max.}$ when

$$\frac{L_S}{D} - \frac{\Delta_{sh}}{D} = \frac{2}{3}\left(\frac{L_s}{D}\right)_{\max.} \tag{16}$$

Together with Eq. (13), Eq. (16) gives

$$S_{L_S}{}^* = 0.26 - 0.024(L_S/D)_{\max.} \tag{17}$$

Combining Eqs. (10) and (17) gives $S_{L_S}{}^*$ as a function of Mach number (Fig. 9). As this $S_{L_S}{}^*$ is for flat-faced cylinders, Fig. 9 represents the maximum Strouhal number for all spike-induced flow pulsations. Figure 5 shows that the deviation from the linear relationship and the associated similar flow assumption, Eq. (13), begins at

$$\frac{L_S}{D} - \frac{\Delta_{sh}}{D} = 0.45\left(\frac{L_S}{D}\right)_{\max.} \tag{18}$$

Letting S_{L_S} reach $S_{L_S}{}^*$ in a smooth high-order fashion for $L_S/D - \Delta_{sh}/D = (L_S/D)_{\max.}$ gives the following modification of Eq. (15):

Figure 10 shows the predictions by Eq. (19), compared with the experimental data.[4-7,25-27] As most of the experimental data fall in the region for which Eq. (13) is valid, $0.25 \leq (L_S/D - \Delta_{sh}/D) \leq 0.45\ (L_S/D)_{\max.}$, the improvement, in agreement between experiment and theory is not very striking when comparing Figs. 8 and 10. However, when considering the frequencies measured on so-called

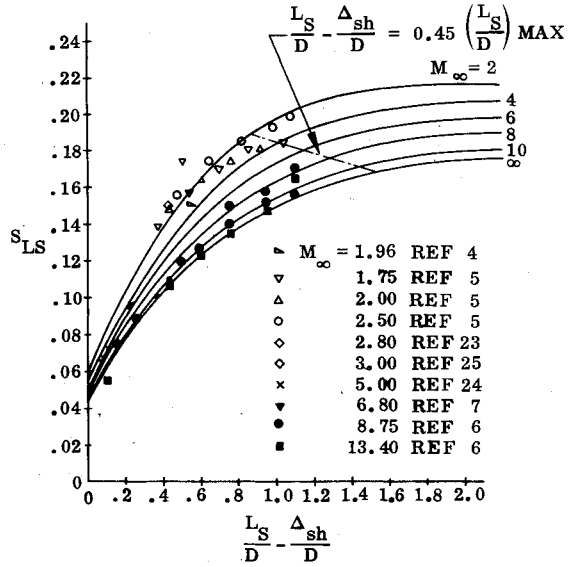

Fig. 10 Comparison between predicted and measured Strouhal numbers.

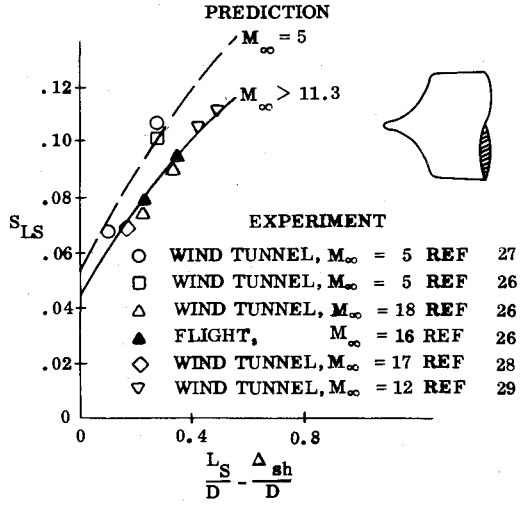

Fig. 11 Flow pulsations on probescidean nose geometries.

$$S_{L_S} = \begin{cases} \frac{0.0556}{X_l^{1/2}}\left[1 + 3.46\left(\frac{L_S}{D} - \frac{\Delta_{sh}}{D}\right)\right] & \left(\frac{L_S}{D} - \frac{\Delta_{sh}}{D} < \frac{1}{4}\right) \\ \frac{0.214}{X_l^{1/2}}\left(\frac{L_S}{D} - \frac{\Delta_{sh}}{D}\right)^{1/2}\left[1 - 0.14\left(\frac{L_S}{D} - \frac{\Delta_{sh}}{D}\right)\right] & \left(\frac{1}{4} \leq \frac{L_S}{D} - \frac{\Delta_{sh}}{D} \leq X_l\right) \\ S_{LS}{}^* - (S_{LS}{}^* - S_{LSI})\left\{\left[\frac{L_S}{D} - \frac{\Delta_{sh}}{D} - \left(\frac{L_S}{D}\right)_{\max.}\right] \Big/ 0.55\left(\frac{L_S}{D}\right)_{\max.}\right\}^n & \left(\frac{L_S}{D} - \frac{\Delta_{sh}}{D} > X_L\right) \end{cases} \tag{19}$$

where

$$S_{LS}{}^* = 0.260 - 0.0535X_l$$

$$S_{LSI} = 0.214 - 0.030X_l$$

$$X_l = 0.45(L_S/D)_{\max.}$$

$$n = -\frac{0.059(L_S/D)_{\max.}(1 - 0.14X_l)}{X_l(S_{LS}{}^* - S_{LSI})}$$

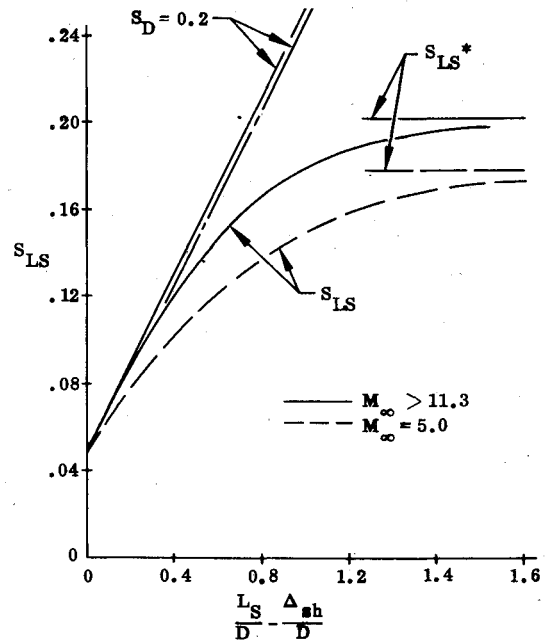

Fig. 12 Limiting Strouhal numbers of spike-induced flow pulsations.

probescidean nose shapes,[26-29] the modification for short spike length is needed. In addition, one has to consider that when the main body face is not flat, but of some convex geometry, an effective spike length $\bar{L}$ can be defined as the axial distance between spike tip and reattachment (see inset in Fig. 6). In this case, the reattachment diameter $\bar{D}$ may also be significantly different from D. Thus, $\bar{L}/\bar{D}$ has to be used instead of L_S/D. Substituting $\bar{L}/\bar{D}$§ for L_S/D in Eq. (19) gives the prediction shown in Fig. 11. The agreement with experimental results[26-29] is very satisfying. Figure 12 finally demonstrates how the Strouhal number $S=0.2$ enters into the picture. It represents the upper limit of the pulsation frequency with the characteristic length being the face diameter for short spikes or probescidean nose shapes and the spike length for long spikes.

Conclusions

A study of the unsteady aerodynamics of bodies with concave nose geometries has produced simple analytic means by which the frequency of the pulsating flow phenomenon occurring at supersonic speeds can be determined. The agreement between predictions and available experimental results is excellent, both in regard to spiked bodies and the so-called probescidean noses. It is found that the Strouhal number $S=0.2$ defines an upper limit for the oscillation frequency, where the characteristic length is the face diameter for short spikes or probescidean nose shapes and the spike length for long spikes.

Acknowledgments

The results presented were obtained in a study for NASA, Contract NAS 8-30652, under the direction of W. W. Clever, NASA Marshall Space Flight Center, and J. C. Young, NASA Johnson Space Center.

References

[1] Chen, K. K., Pallone, A. J., and Thyson, N., "Types of Nose Tip Shape Change During Atmosphere Entry," presented at AIAA 7th Fluid and Plasma Dynamics Conference, Palo Alto, Calif., June 1971.

[2] Kabelitz, H-P., "Zur Stabilität geschlossener Grenzschichtablösegebiete an Konischen Drehkörpern bei Hyperschallanströmung," DLR FB 71-77, July 1971.

[3] Kabelitz, H-P., "Zur Stabilität geschlossener Grenzschichtablösegebiete bei Über-und Hyperschallanströmung," Vertrags-Nr. 71-065, 4. Jahrestagung der D6LR, Baden-Baden, W. Germany, Oct. 1971.

[4] Mair, W. A., "Experiments on Separation of Boundary Layers on Probes in Front of Blunt-Nosed Bodies in a Supersonic Air Stream," *Philosophical Magazine*, Vol. 43, July 1952, pp. 695-716.

[5] Daniels, L. E. and Yoshihara, H., "Effect of the Upstream Influence of a Shock Wave at Supersonic Speeds in the Presence of a Separated Boundary Layer," Wright Air Development Center, Wright Patterson AFB, Ohio, WADC TR No. 54-31, Jan. 1954.

[6] Kabelitz, H-P, Wyborny, W., and Schepers, II-J., "Untersuchungen über den Wärmeübergang am Zentralstift von stumpfen Körpern," DLR Mit. 67-13, 1967, pp. 92-124.

[7] Maull, D. J., "Hypersonic Flow over Axially Symmetric Spiked Bodies," *Journal of Fluid Mechanics*, Vol. 8, Part 4, Aug. 1960, pp. 584-594.

[8] Elfstrom, G. M., "Turbulent Separation in Hypersonic Flow," Imperial College, London, Aero Rept. 71-16, Sept. 1971.

[9] Settles, G. S., Bogdonoff, S. M., and Vas, I. E., "Incipient Separation in Supersonic Turbulent Boundary Layer," AIAA Paper 75-7, 13th Aerospace Sciences Meeting, Pasadena, Calif., Jan. 1975.

[10] Holden, M. S., "Shock Wave-Turbulent Boundary Layer Interaction in Hypersonic Flow," AIAA Paper 72-74, 10th Aerospace Sciences Meeting, San Diego, Calif., Jan. 1972.

[11] Reding, J. P. and Ericsson, L. E., "Effects of Delta Wing Separation on Shuttle Dynamics," *Journal of Spacecraft and Rockets*, Vol. 10, July 1973, pp. 421-428.

[12] Reding, J. P. and Ericsson, L. E., "Review of Delta Wing Space Shuttle Dynamics," Space Shuttle Technology Conference, Vol. III – Aerodynamics, NASA TMX-2508, Feb. 1972, pp. 861-921.

[13] Reding, J. P. and Ericsson, L. E., "Review of Delta Wing Space Shuttle Vehicle Dynamics," NASA CR 115357, Oct. 1971.

[14] Ames Research Staff, "Equations, Tables, and Charts for Compressible Flow," NACA Rept. 1135, 1953.

[15] Ericsson, L. E. and Reding, J. P., "Unsteady Aerodynamic Flow Field Analysis of the Space Shuttle Configuration, Part III: Unsteady Aerodynamics of Bodies with Concave Nose Geometries," NASA CR-144334, April 1976.

[16] Eggers, A. J. and Hermach, C. A., "Initial Experiments on the Aerodynamic Cooling Associated with Large-Scale Vortical Motions in Supersonic Flow," NACA RM A54L13, March 1955.

[17] Ericsson, L. E. and Reding, J. P., "Analysis of Flow Separation Effects on the Dynamics of a Large Space Booster," *Journal of Spacecraft and Rockets*, Vol. 2, July-Aug. 1965, pp. 481-490.

[18] Ericsson, L. E. and Reding, J. P., "Dynamics of Separated Flow over Blunt Bodies," NASA CR-76912, Nov. 1962.

[19] Chapman, D. R., Kuehn, D. M., and Larson, H. K., "Investigation of Separated Flows in Supersonic and Subsonic Streams with Emphasis on the Effects of Transition," NACA Rept. 1356, 1958.

[20] Serbin, H., "Supersonic Flow Around Blunt Bodies," *Journal of Aerospace Sciences*, Vol. 25, Jan. 1958, pp. 58-59.

[21] Chapman, D. R., Mark, H., and Pirtle, M. W., "Computers Versus Wind Tunnels for Aerodynamic Flow Simulations," *Astronautics and Aeronautics*, Vol. 13, April 1975, pp. 22-29.

[22] Roache, P. J. and Bradshaw, P., (letters in response to Ref. 21) *Astronautics and Aeronautics*, Vol. 13, Sept. 1975, pp. 4-6.

[23] Kutterer, R. E., "Pulsationen der Strömung um Klugkörper," ISL-Kolloquim 8/60, 1960.

[24] Abbett, M. J., Cooper, L., Dahm, T. J., and Jackson, M. D., "Flow Characteristics about Concave Conic Forebodies at High Mach Numbers," AIAA Paper 75-153, Pasadena, Calif., Jan. 1975.

[25] Demetriades, A., private communication and informal data presented at the Second Boundary Layer and Shape Change Interchange Meeting, Aerospace Corporation, El Segundo, Calif., May 1974.

[26] Cassanto. J. M., Monfort, A., and Fehl, C., "An Experiment to Determine the Existence of R/B Nosetip Transient Shocks," AIAA Paper 76-54, Washington, D. C., Jan. 1976.

[27] Baltakis, F. P., "Wind-Tunnel Study of Oscillating Flow-Induced Surface Pressures on a Tension-Cone Geometry Model," Naval Ordnance Laboratory, NOL TR 74-134, Jan. 1974.

[28] Kenworthy, M. A. and Richard, B. E., "A Study of the Unsteady Flow Over Concave Conic Models at Mach 15 and 20," Air Force Materials Laboratory, AFML-TR-75-138, Oct. 1975.

[29] Reeves, B. L., private communication of unpublished results, Nov. 1975.

§Computed for tangential reattachment (see discussion of Eq. (11)).